Naval Research Laboratory

Washington, DC 20375-5320

Effects of Loading and Doping on Iron-based CO₂ Hydrogenation Catalysts

ROBERT W. DORNER

NRC Postdoctoral Research Associate
Navy Technology Center for Safety and Survivability
Chemistry Division

HEATHER D. WILLAUER
DENNIS R. HARDY
FREDERICK W. WILLIAMS

Navy Technology Center for Safety and Survivability
Chemistry Division

August 24, 2009

REPORT DOCUMENTATION PAGE

1. REPORT DATE *(DD-MM-YYYY)* 24-08-2009	2. REPORT TYPE Memorandum Report	3. DATES COVERED *(From - To)*

4. TITLE AND SUBTITLE

Effects of Loading and Doping on Iron-based CO_2 Hydrogenation Catalysts

5a. CONTRACT NUMBER

5b. GRANT NUMBER

5c. PROGRAM ELEMENT NUMBER

6. AUTHOR(S)

Robert W. Dorner,* Heather D. Willauer, Dennis R. Hardy, and Frederick W. Williams

5d. PROJECT NUMBER

5e. TASK NUMBER

5f. WORK UNIT NUMBER

7. PERFORMING ORGANIZATION NAME(S) AND ADDRESS(ES)

Naval Research Laboratory, Code 6183
4555 Overlook Avenue, SW
Washington, DC 20375-5320

8. PERFORMING ORGANIZATION REPORT NUMBER

NRL/MR/6180--09-9200

9. SPONSORING / MONITORING AGENCY NAME(S) AND ADDRESS(ES)

Naval Facilities Engineering Service Center
1100 23rd Avenue
Port Hueneme, CA 93043-4370

10. SPONSOR / MONITOR'S ACRONYM(S)

11. SPONSOR / MONITOR'S REPORT NUMBER(S)

12. DISTRIBUTION / AVAILABILITY STATEMENT

Approved for public release; distribution is unlimited.

13. SUPPLEMENTARY NOTES

*NRC Postdoctoral Research Associate

14. ABSTRACT

Hydrogenation of CO_2 to hydrocarbons is investigated over γ-alumina iron-based catalysts to produce unsaturated hydrocarbons as feedstock chemicals for jet-fuel synthesis. It is shown that conversion levels up to 38% can be achieved by doping the iron with Mn. Furthermore, it was possible to obtain an olefin/paraffin ratio of over 1.16. The doping levels played a crucial role in the product distribution as well as CO_2 conversion yields, with over doping leading to suppression of the desirable hydrocarbon products. Characterization of the catalysts by XRD, XPS, and SEM shed light on the role each dopant had on the overall catalyst's activity and production distribution.

15. SUBJECT TERMS

Iron catalyst	Olefin/paraffin ratio	Manganese
CO_2 hydrogenation	γ-alumina	

16. SECURITY CLASSIFICATION OF:			17. LIMITATION OF ABSTRACT	18. NUMBER OF PAGES	19a. NAME OF RESPONSIBLE PERSON Heather D. Willauer
a. REPORT Unclassified	**b. ABSTRACT** Unclassified	**c. THIS PAGE** Unclassified	UL	16	19b. TELEPHONE NUMBER *(include area code)* (202) 767-2673

i

CONTENTS

EFFECTS OF LOADING AND DOPING ON IRON-BASED CO$_2$ HYDROGENATION CATALYSTS

1.0   BACKGROUND

There is an interest within the US Department of Defense (DOD) to certify, develop, and use synthetic fuel from renewable resources. These fuels are not only considered CO$_2$ neutral they have the additional potential benefits of providing a viable avenue for reducing dependence on increasingly expensive fossil fuels and reducing fuel logistic tails and their vulnerabilities.

DOD is the single largest buyer and consumer of fuel using approximately 12.6 million gal per day [1]. Approximately 11 million gal per day is jet fuel (note the term jet fuel includes use in both aircraft and ground vehicles) and the remainder is shipboard marine distillate (all Navy and Marine Corps use). Furthermore, the cost per gallon paid by the DOD is $4 per gallon, which amounts to over $18 billion annually. This figure does not include logistical procurement and transportation of the fuel [1, 2].

With strongly fluctuating fuel prices and 'peak oil' production expected to occur in 2010 to 2025+ (by some experts' estimates, we already reached peak production in 2004) [3, 4] it would be highly desirable to develop a way to reduce the financial strain on the DOD, by producing synthetic hydrocarbon (HC) fuel from completely non-fossil fuel sources and processes. Production of this synfuel could be performed at sea, which would furthermore alleviate the need of transporting the fuel for many miles to the point of use. However, the produced fuel also needs to meet military requirements called Battlefield Use Fuel of the Future (BUFF); most importantly it must have a maximum freezing point of -47 °C, and a minimum flashpoint of 60 °C [5]. Thus, the DOD has a vested interest in supporting the development of synthetic fuel from the vast natural resources such as gas hydrates, and CO$_2$ available in the United States [6].

Technologies currently exist to synthesize synfuel on land, applying gasification of carbon-containing feedstock, such as coal and biomass. However, these technologies are not practical for sea-based fuel production. The approach within relies totally on the utilization of carbon sources available in seawater in combination with hydrogen to produce synthetic hydrocarbon fuel. This synfuel process would be CO$_2$ neutral and provide an alternative energy source to fossil fuels. Thus such a process could directly benefit the U.S. Navy.

2.0   INTRODUCTION

Even though CO$_2$ is a ubiquitous and relative abundant available carbon source, the problem with its use is its great chemical stability. Besides being a possible carbon source and building block for the production of more energy-rich molecules, CO$_2$ is also well known to have a detrimental impact on global warming [7]. Many different technologies have been proposed to reduce its impact on global warming such as geological sequestration. This entails capturing the CO$_2$ released by burning fossil fuels and subsequent sequestration into geologic formations. However, an interesting and attractive alternative to storing CO$_2$ through sequestration would be

the recycling of the gas into energy-rich compounds. Its potential as a chemical feedstock for the production of valuable hydrocarbons is therefore of great interest [8].

Due to the increased awareness of the impact CO_2 is having on weather, rising sea-levels and other natural catastrophes, the R&D efforts to bind CO_2 has seen an immense increase in attention over the last few years. Proposals range from CO_2 capture from the atmosphere, binding it in CaO using solar energy [9], to converting CO_2 to hydrocarbons over catalysts, either photocatalytically, electrocatalytically or thermochemically. Electrochemical and photochemical CO_2 conversion is still in its research infancy and has major drawbacks at present. Photocatalysts tend to need a sacrificial electron donor [10, 11] and neither photocatalytic or electrocatalytic conversion yields long chain products or show very high CO_2 conversion efficiencies [12]. Thermochemical CO_2 conversion has been known for several decades [13] and is presently the most proven and successful approach in producing a greater yield of hydrocarbon (HC) products above methane. The use of traditional Fischer-Tropsch synthesis (FTS) cobalt catalysts has shown very little affinity in forming long chain hydrocarbons due to their low water-gas-shift (WGS) ability. Instead they mainly function as a methanation catalyst [14]. Iron based catalyst have shown much more promise at hydrogenating CO_2 [15]. However, to obtain higher CO_2 conversion efficiencies and greater selectivity and yield in desired hydrocarbon products further research is needed in developing, modifying, characterizing and understanding these catalysts.

This work describes CO_2 hydrogenation by iron based catalysts. The effect of iron loading and surface modification on the catalyst by the addition of manganese on product selectivity and CO_2 conversion is discussed. Spectroscopic techniques are used to analyze and interpret how each component changed the surface characteristics of the catalyst and thus the overall catalyst performance.

3.0   EXPERIMENTAL

3.1 Catalyst Preparation

Gamma alumina (Matheson Coleman & Bell) with a surface area and pore radius of 218.3 m^2/g and 1.2 to 3.7 nm, respectively, was used as support material. A co-incipient wetness impregnation (IWI) method was used for catalyst preparation. $Fe(NO_3)_3 \cdot 6H_2O$ (Aldrich), $KMnO_4$ (Aldrich), KNO_3 (Aldrich) and alumina were added to a flask containing 50ml of deionized water at the concentrations required to obtain the desired Mn/Fe and K/Mn/Fe weight ratios, resulting in a solid between 10-15 grams. These impregnated samples were then dried at 373K in air. Finally, the catalysts were calcined at 623K for 16 hours, under static air conditions.

3.2 Catalyst Testing and Characterization

All CO_2 hydrogenation reactions with the catalyst described within were conducted in a 1 L Parr Continuously Stirred Tank Reactor (CSTR). Upon completion of the hydrogenation reactions, the catalyst properties were characterized by a series of spectroscopic techniques (XRD, XPS, SEM, and BET) described below.

2

3.2.1 Continuously Stirred Tank Reactor (CSTR) Set-Up

In a typical CO_2 hydrogenation experiment, 10-15 g of calcined catalyst were dispersed in approximately 400 ml of mineral oil (Aldrich) in the CSTR and subsequently reduced in-situ using CO at 290°C for 48 h.

Two mass flow controllers regulated by an MKS 647C multigas controller, were used to adjust the flow rate of CO_2 and H_2. Hydrogenation of CO_2 was conducted at 290 °C, 200 psig and a gas hourly space velocity (GHSV) of 1400 h^{-1} at a H_2:CO_2 ratio of 3:1. The effluent gases were analyzed online using a Varian CP-3800gas chromatograph (GC) equipped with a SP-1700 packed column and a thermal conductivity detector. The SP-1700 column only separates HC up to C_6. The pressure in the reactor was kept constant by placing a Tescom dome-loaded backpressure regulator between the reactor and the GC (see Figure 1 for reactor set-up). Time-on-stream (TOS) for all catalysts was 100 hours.
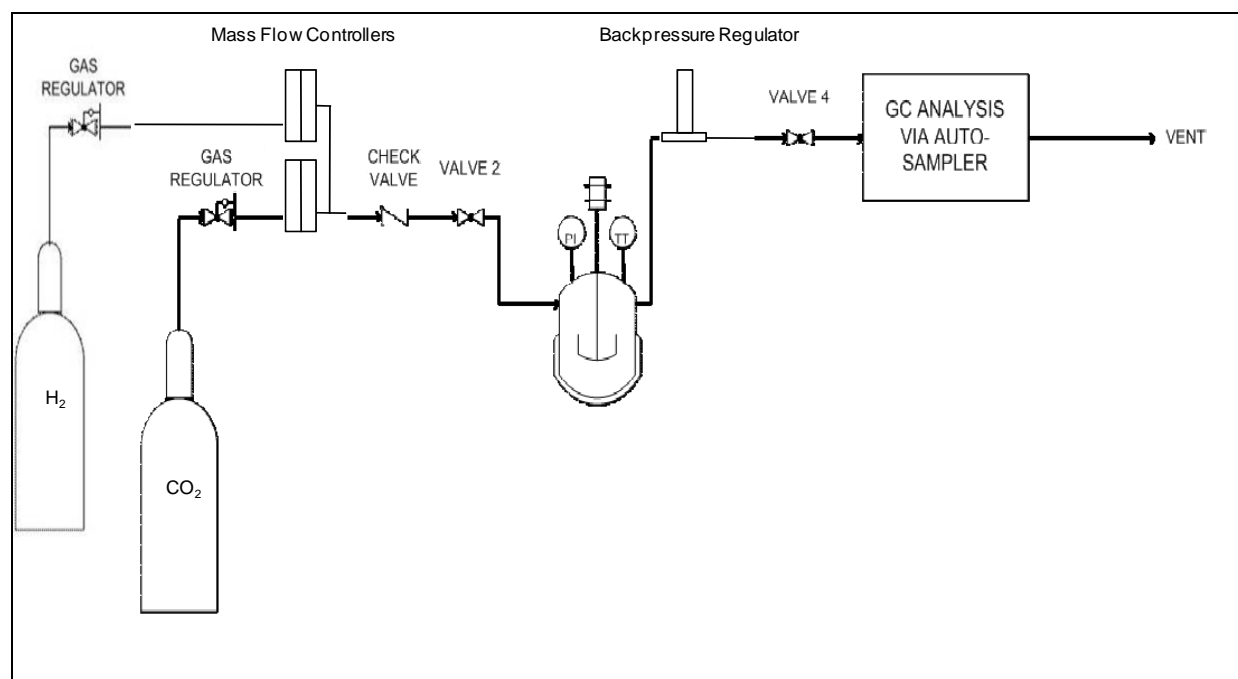
Figure 1. Reactor set-up

3.2.2 Powder X-Ray Diffraction (XRD)

Powder XRD measurements were performed on all catalyst materials. The catalyst was dissolved in heptane before XRD measurements were taken, to remove the mineral oil from the solids. The catalyst was subsequently recovered by conventional filtering procedures. The data were collected on a D8 Siemens Bruker diffractometer with a general area detector employing the Bragg-Brentano geometry and the $CuK_{\alpha}1$ wavelength. The data were collected in the 15-50° 2θ range with a step increment of 0.01° and the time for each step was 2s. The data were visualized and indexed using the celref3 software [16].

3

3.2.3 X-ray photoelectron spectroscopy (XPS)

XPS was used to assess the surface species and quantities present on the powder particles. The XPS studies were carried out using a K-Alpha machine (Thermo Scientific, UK) and the Unifit software [17] for data analysis. The system's base pressure was less than 5×10^{-9} mbar, however the pressure in the analysis chamber during data collection and analysis was 2×10^{-8} mbar due to the use of the low-energy electron flood gun for charge neutralization. A monochromated Al Kα (hν = 1456.6 eV) was used as the x-ray source.

3.2.4 Scanning Electron Microscope (SEM)

Structural and chemical characterization was performed with a field emission scanning electron microscope (FESEM) - Model LEO DSM 982, LEO. The SEM was operated at an accelerating voltage of 5 kV and the working distance varied from 3 to 8 mm. The powder was placed under the SEM detector as a loosely scattered powder stuck to conducting tape.

3.2.5 BET surface area measurements

BET surface areas were measured using a Micromeritics ASAP2010 accelerated surface area and porosimetry system. An appropriate amount (~0.25 g) of catalyst sample was taken and slowly heated to 200 ^{o}C for 10 h under vacuum (~50 m Torr). The sample was then transferred to the adsorption unit, and the N_2 adsorption was measured at the boiling temperature of nitrogen.

4.0   RESULTS AND DISCUSSION

Based on previous work done by our group [14] it is apparent that direct hydrogenation of CO_2 over a general Cobalt-based FTS catalyst (namely Co-Pt/Al$_2$O$_3$), mainly yields methane as a product, which is unsuitable for direct use as jet-fuel. Our current approach is to create a two-stage synthesis process for the conversion of CO_2 to jet-fuel. This entails the hydrogenation of CO_2 to olefins over modified iron based FTS catalysts, which will then be followed by oligomerization to jet-fuel over solid-acid catalysts. When used for the hydrogenation of CO_2, iron based catalysts show a high tendency to form unsaturated HC, especially when doped with Mn and/or K [15, 18-20]. We therefore decided to synthesize, test and characterize Fe, Mn and K catalysts supported on alumina in efforts to optimize the loading of the catalyst's components in efforts to increase hydrocarbon product selectivity and yield.

Initially, the optimum iron loading was established by testing three different catalysts, with 9, 17 and 25 weight percent (% w/w) iron dispersed over the γ-alumina support. Tables 1 and 2 show when the active catalytic component was increased from 9 to 17 % w/w, the CO_2 conversion increased drastically, almost linearly with the increase in metal deposited. However, when the metal loading was further increased to 25 % w/w, the CO_2 conversion stagnates and only increased marginally in comparison to the catalyst containing 17 % w/w Fe. All catalytic materials showed roughly the same product distribution, with approximately 50% of the product being methane, 35% C_2-C_{5+} and the remainder being 15% CO. Within the C_2-C_{5+} range the olefin to paraffin ratio was about 0.25 for all catalysts (Tables 1 and 2). Thus the 17 % w/w

showed the greatest promise of CO_2 conversion. The relative decrease in CO_2 conversion over the 25 % w/w Fe catalyst is elucidated when looking at the respective XRD patterns of the different % w/w iron catalysts (see Figure 2).
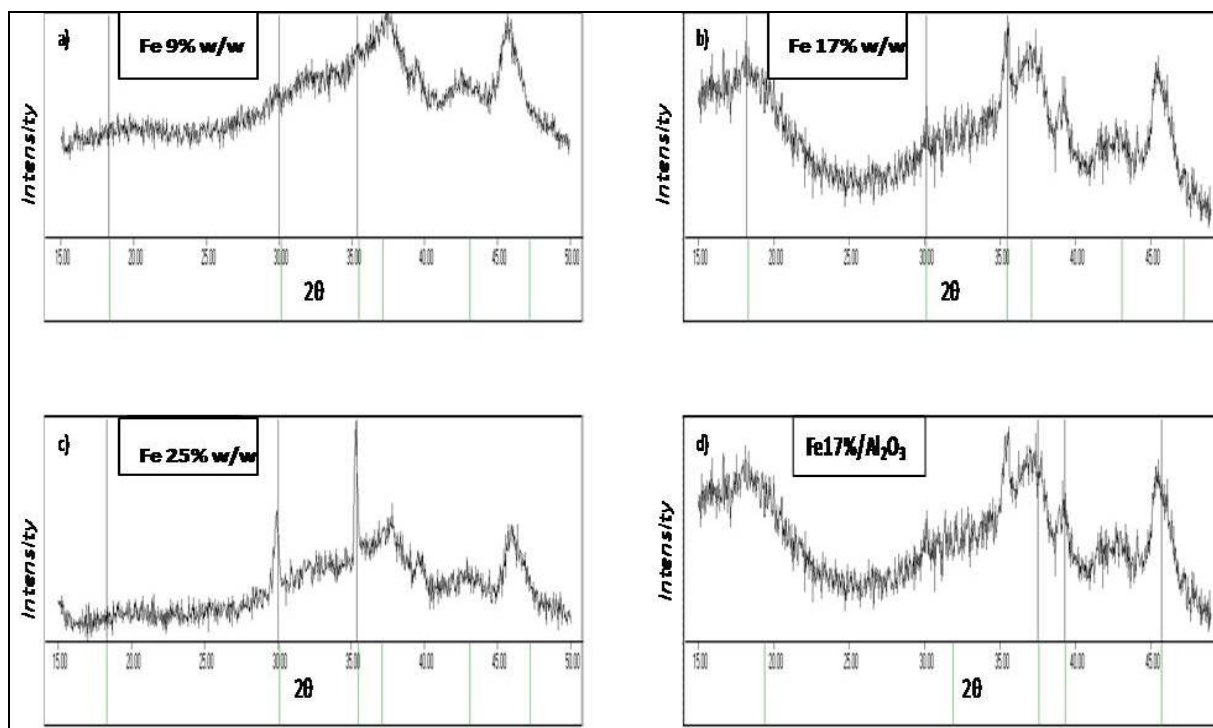

Figure 2. XRD patterns of Fe 9 % w/w, 17 % w/w and 25 % w/w dispersed on Al_2O_3. Indexing of the Fe_3O_4 phase is shown at the bottom of the diagrams a) – c). Diffraction peaks of Fe_3O_4 become more visible and more intense with increasing Fe-loading. The γ-alumina is indexed in diagram d) for phase identification and full peak assignment.

Neither the 9 % w/w nor the 17 % w/w Fe catalyst showed any clear signs of bulk formation. However, the 25 % w/w Fe catalyst displays very apparent Fe_3O_4 diffraction peaks, thus indicating the formation of bulk Fe_3O_4 crystallites being formed in preference over uniformly dispersed nanoparticles on top of the alumina support [21]. Both the 9 % w/w and the 17 % w/w seem to have a very good dispersion of nano-sized particles over the support. SEM images of the 17 % w/w Fe catalyst indeed show 100 nm particles dispersed over the alumina support while the SEM image of Fe 25 % w/w clearly indicates a significant increase in particle size, 200 nm (see Figure 3).
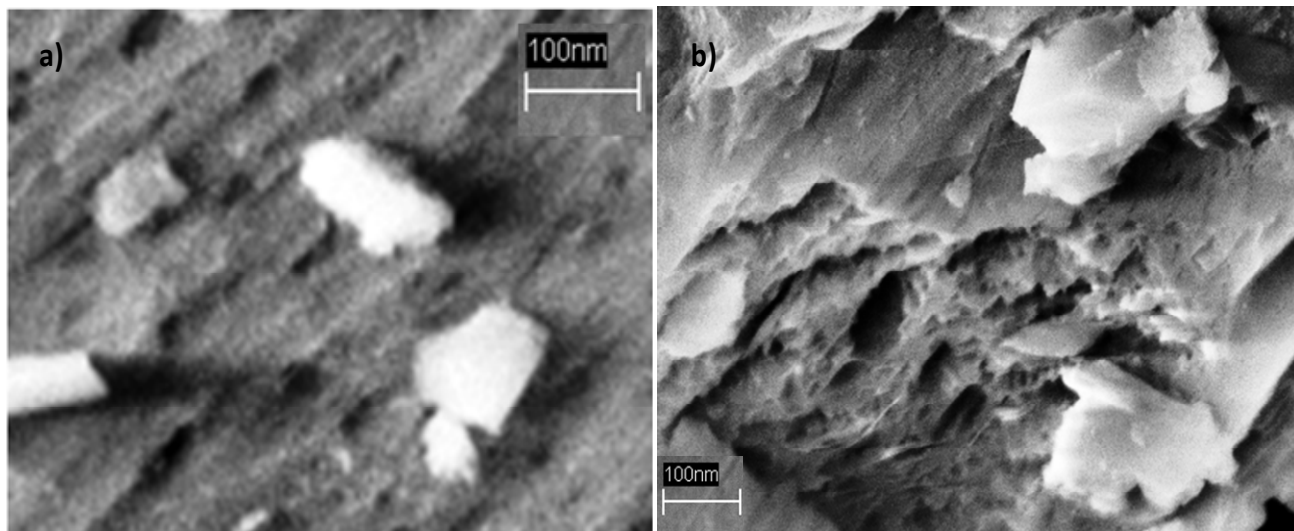
Figure 3. SEM images of a) Fe 17 % w/w / Al$_2$O$_3$, showing dispersion of ca. 100 nm sized nano-particles and b) Fe 25 % w/w / Al$_2$O$_3$, showing dispersion of ca. 200 nm sized nano-particles.

The SEM images corroborate, that the relative decrease in CO$_2$ conversion with increasing weight percentage of iron above 17 % is due to the increase in particle size. This suggests there is a decrease in active site availability/weight unit of iron as was suggested by the presence of clearly defined XRD diffraction peaks at the higher iron loading. Interestingly, besides indicating an increase in particle size with increasing iron loading above 17 % w/w, the XRD patterns infer there is a magnetite phase (Fe$_3$O$_4$) and several different iron carbide phases (Fe$_X$C$_Y$) present [22] (see Figure 4). In addition, the patterns also reveal there is no hematite phase (Fe$_2$O$_3$) nor metallic iron present.
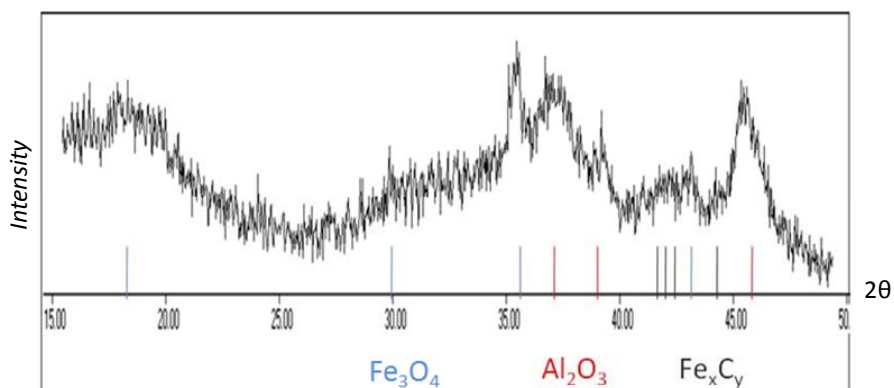
Figure 4. XRD pattern of Fe 17 % w/w / Al$_2$O$_3$, showing the presence of Fe$_X$C$_Y$ phases besides magnetite and alumina.

It has been postulated, that while the magnetite phase is responsible for the water gas shift activity in iron catalysts used for FTS [23], the carbide phase is essential in FTS for chain growth [24-26]. This has been shown by changing the reducing agent of the fresh catalyst from CO to H$_2$ and subsequently observing a lower CO conversion [22].

Having established the optimum iron loading of the catalyst to be 17 % w/w, Mn was subsequently co-precipitated with iron at different loadings, ranging from 4 % w/w to 20 % w/w. Mn has been shown to suppress methane formation and increase the olefin/paraffin ratio in FTS as well as CO_2 hydrogenation [18]. Abbot et al. proposed that Mn acts as an electronic as well as a structural promoter, leading to an increase of Fe dispersion over the Al_2O_3 support [27]. Li et al. suggested that Mn promotes catalyst reduction, the dispersion and carburization of Fe_2O_3, while also greatly increasing the catalyst surface basicity and thus suppressing the formation of CH_4 in favor of longer chain hydrocarbons [28].

Indeed Tables 1 and 2 show that with a doping level of 4 % w/w of Mn, it is already possible to drastically favor the long chain HC fraction over methane. Along with the shift to longer chain HC, the olefin/paraffin ratio is also increased, while the overall CO_2 conversion increases marginally. An even greater increase in longer chain HC and the olefin-to-paraffin ratio can be observed at a Mn loading of 12 % w/w. At this loading the methane fraction of the products is reduced by approximately 20%, while the olefin/paraffin ratio almost increases by a factor of 5 for an overall CO_2 conversion rate of 37.71%. Raising the Mn loading further to 20 % w/w causes both the CO_2 conversion and the olefin/paraffin ratio to decrease and the methane product distribution to return to levels seen with 4 % w/w Mn. Interestingly however the CO fraction of the products increases from 10.67 to 15.64% upon increasing the Mn loading (see Table 1 and 2 for the catalysts' conversion yields and product distribution).

Table 1. Product selectivity, olefin/paraffin ratio and CO_2 conversion over several different Fe 17 % w/w / Al_2O_3 based catalysts.

Catalyst	Selectivity (%, carbon base)			Olefin/Paraffin	CO2 Conversion
	C1	C2-C5+	CO yield		(%)
Fe 9%	55.09	34.85	10.06	0.25	18.21
Fe 17%	54.93	35.07	10.00	0.25	29.22
Fe 25 %	54.89	35.13	9.98	0.25	32.15
Mn 4% Fe 17%	42.03	46.47	11.50	0.68	34.43
Mn 12% Fe 17%	34.01	55.32	10.67	1.16	37.71
Mn 20% Fe 17%	40.75	43.44	15.82	0.95	25.94

**Table 2.** Breakdown of CO_2 conversion products, including olefin/paraffin ratios for C_2-C_4.

Catalyst	Selectivity (%, carbon base)						C2 Ol/Par	C3 Ol/Par	C4 Ol/Par
	C1	C2	C3	C4	C5+	CO			
Fe 9%	55.09	30.75	1.83	1.51	0.76	10.06	0.72	0.39	0.35
Fe 17%	54.93	30.99	1.8	1.52	0.76	10	0.72	0.39	0.35
Fe 25 %	54.89	31.03	1.83	1.5	0.77	9.98	0.72	0.39	0.35
Mn 4% Fe 17%	42.03	42.31	1.91	1.49	0.76	11.50	0.72	0.39	0.35
Mn 12% Fe 17%	34.01	44.23	6.56	3.94	0.59	10.67	1.08	2.84	0.91
Mn 20% Fe 17%	40.75	34.73	4.30	3.58	0.83	15.82	0.99	1.82	0.49

Figure 5 compares the XRD patterns obtained for catalysts containing 12 % w/w Mn and 20 % w/w Mn. β-MnO_2 diffraction peaks are observed for both samples; however the higher Mn-

loading displays much clearer and distinct diffraction peaks, indicating larger crystallites. At lower Mn loadings a good dispersion of the metal centers can be inferred.
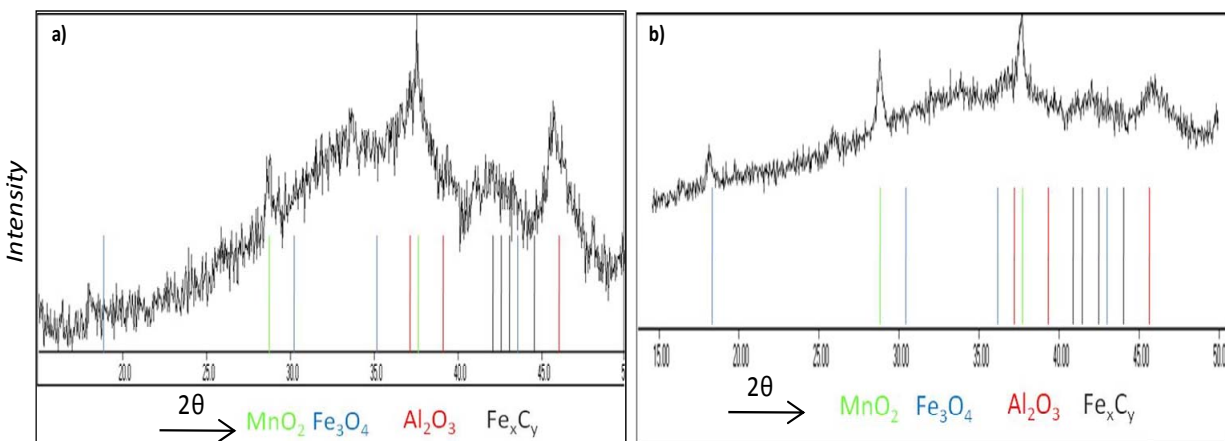
Figure 5. XRD pattern of a) Mn12 % w/w Fe17 % w/w / Al_2O_3 and b) Mn 20 % w/w Fe17 % w/w / Al_2O_3, showing the presence of bulk MnO_2 formation upon Mn doping levels of 20 % w/w. All species are indexed for peak assignment clarity.
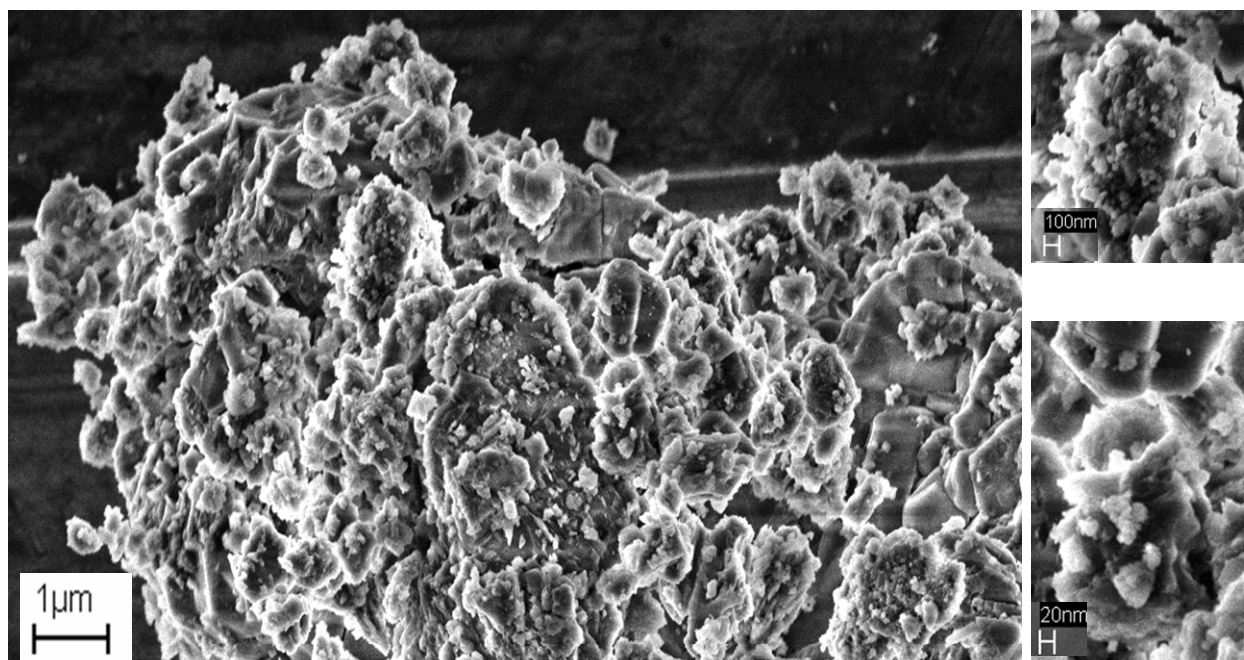
Figure 6. SEM image of Mn 12 % w/w Fe 17 % w/w / Al_2O_3, showing a good dispersion of nano-particles on the alumina. The average particle size seems to range from 20 to 100nm and is thus smaller than with the Fe 17 % w/w catalyst.

SEM images taken of this catalyst show a good dispersion and also a reduction in particle size when compared to the undoped iron catalyst (see Figure 6). Besides leading to a quite significant reduction in CO_2 conversion when increasing the Mn loading to 20 % w/w, one can

also see a clear reduction in longer chain HC being formed in favor of methane (Tables 1 and 2). Thus over doping of the iron catalyst seems to lead to the Mn being deposited not only on the CO_2 hydrogenation site but also on the chain growth site. Furthermore, when the iron catalyst is over-doped (i.e. 20 % w/w), the CO product percentage increases considerably. This is a consequence of the chain growth site being blocked by the Mn particles. Since this prevents CO from being adsorbed and converted to HC, the percentage of CO in the effluent increases.

XPS studies were undertaken to substantiate these assumptions. Initially the Fe 17 % w/w/ Al_2O_3 catalyst was characterized to use as a benchmark and calibration. The Fe and Al 2p photoelectron signal were chosen for analyses. The catalyst make-up was determined to be 17.1 % w/w Fe and 82.9 % w/w Al from the XPS intensities (see Table 3 for XPS intensity data).

Table 3. XPS data, showing peak assignment, area under the curve (measured in at. %) and correlated weight %.

		Peak Assign.	BE (eV)	Area	w%	Total
Fe 17 / Al2O3	Fe 2p	FexCy	709	3.00	3.22%	17.11%
		Fe2+	710.9	6.56	7.05%	
		Fe3+	712.7	6.36	6.83%	
	Al 2p	Al2O3	74.38	159.86	82.89%	82.89%
Mn12 / Fe17 / Al2O3	Fe 2p	FexCy	709	3.23	3.23%	12.96%
		Fe2+	710.8	6.16	6.17%	
		Fe3+	712.5	3.55	3.55%	
	Al 2p	Al2O3	73.98	167.98	81.11%	81.11%
	Mn 2p	MnO2	640.7	6.03	5.93%	5.93%
Mn20 / Fe17 / Al2O3	Fe 2p	FexCy	709	1.44	1.59%	4.74%
		Fe2+	710.8	1.81	2.00%	
		Fe3+	712.5	1.03	1.14%	
	Al 2p	Al2O3	73.98	160.02	85.42%	85.42%
	Mn 2p	MnO2	640.7	9.04	9.84%	9.84%

When the Fe 17 % w/w catalyst contains 12 % w/w Mn, Table 4 shows the Fe surface species is decreased from 17 % w/w to 13 % w/w, with 81.1 % w/w Al and 5.9 % w/w Mn (obtained from the Mn 2p signal) making up the difference. The decrease in the Fe surface species indicates a partial layer of Mn being formed on top of the Fe particle; however the small decrease as well as the below expected Mn surface species present, indicates that a large part of the Mn dopant is incorporated within the Fe particles. This suggests that besides being a structural promoter (i.e. increase in dispersion and hydrogenation prohibition), Mn may also act as an electronic promoter as previously suggested by Abbot et al. for FTS catalysts [27].

While comparing the XPS spectra obtained from the Mn 20 % w/w/ Fe 17 % w/w catalyst a clear difference is observed (Table 3). The Fe 2p signal is strongly attenuated indicating a surface make up of 4.7 % w/w Fe, 9.9 % w/w Mn and 85.4 % w/w Al. It can be clearly seen that Mn has formed an over layer on top of the iron, leading to a suppression of the Fe 2p photoelectron

signal. This decrease in surface iron through the deposition of a Mn surface layer at 20 % w/w is visualized when plotting XPS Fe 2p intensity v. Mn loading as shown in Figure 7.
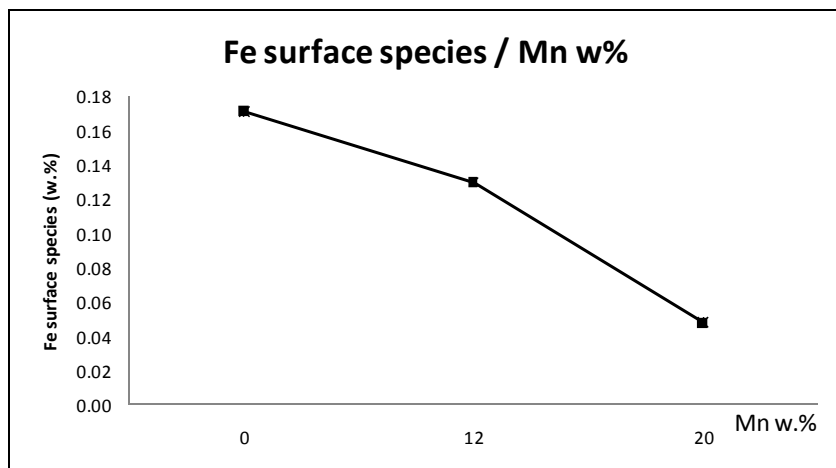

Figure 7. Depiction of XPS Fe 2p intensity v. Mn loading. A loading of 20 % w/w Mn leads to a severe reduction in Fe surface species.

Once the manganese doping level of the catalyst reaches 20 % w/w, a significant reduction in surface Fe is observed. However the partial reduction in surface Fe-species at a 12 % w/w Mn doping level is clearly beneficial to CO_2 hydrogenation as shown in Tables 1 and 2.

The Fe 2p signal for each catalyst shown in Table 3, when de-convoluted, consists of three different peaks as shown in Figure 8. These peaks can be assigned to the Fe^{3+} and Fe^{2+} ion in the magnetite as well as one signal probably arising from iron carbide based on their chemical shift (Table 3. Binding energies (BE) of 712.5eV, 710.8, and 709.2 respectively – see Figure 8 for XPS spectra) and correlate well with data reported elsewhere [29]. Surprisingly the Fe^{3+}/Fe^{2+} ratio shown in Table 3 does not equal 2 as one would expect from the magnetite's bulk make-up, indicating that the Fe^{2+} species is much more abundant on the metal's surface.
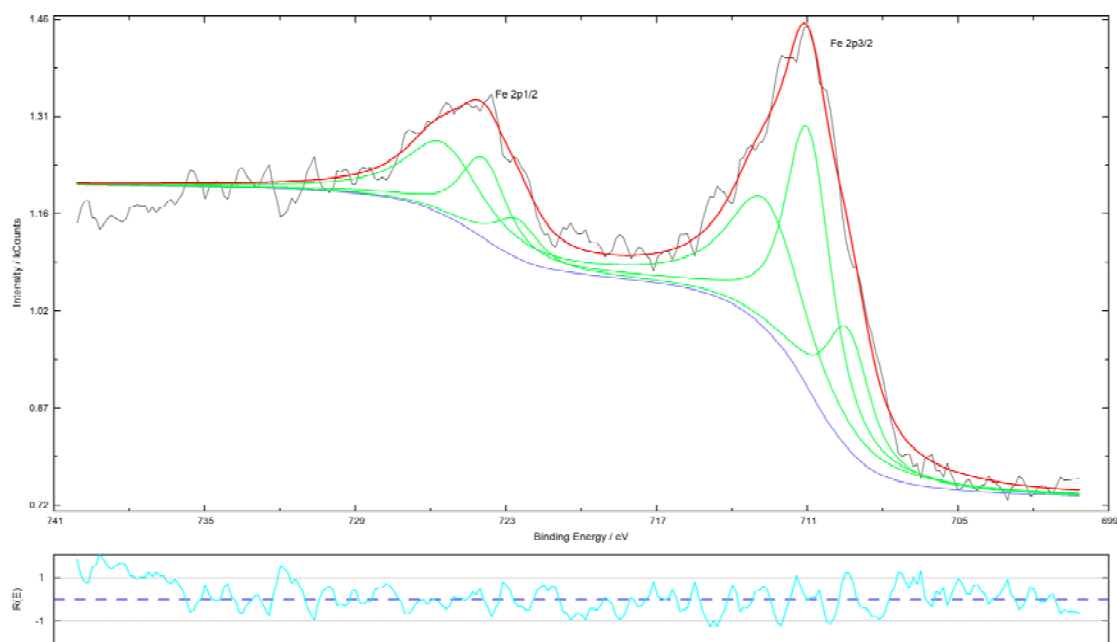
Figure 8. Fe 2p XPS peaks for catalyst shown in Table 3 indicate the presence of three different Fe species, namely Fe^{3+}, Fe^{2+} and Fe_XC_Y.

5.0 CONCLUSIONS

The need for alternative energy sources is becoming ever more important with the rising costs of crude oil and the inevitable reality of peak-oil. The recycling of CO_2 by its conversion to fuel, would result in neutral CO_2 emissions by the fuel. A promising iron-based catalyst has been developed and characterized that can achieve CO_2 conversion levels up to ca. 38%, with an olefin/paraffin ratio of 1.16 (Table 1). XRD, SEM, and XPS analysis were used to determine and explain the role that iron loading and manganese doping had on the product selectivity and CO_2 conversion efficiency.

Iron loading was established at 17 % w/w as a result of the reduction in surface active sites available per unit weight of iron.   The addition of 12 % w/w Mn led to a significant improvement in CO_2 conversion, resulting in an increase in unsaturated higher-chain HC favored over methane and alkane formation. This is the result of Mn being deposited on the iron's hydrogenation active site. Mn was also shown to reduce the particle sizes of the nano-dispersed metal centers on the support. Further catalyst doping with Mn led to the blocking of the catalyst's hydrogenation site causing the CO product percentage to increase from 11% to 16%.

Having established that the optimum iron and manganese catalyst loading on an alumina support as 17 % w/w and 12 % w/w respectively, (Table 1) further catalyst development will be pursued to improve both the olefin/paraffin ratio and CO_2 conversion efficiencies in efforts to produce a catalyst for commercial CO_2 conversion to valuable fossil fuel free HC.

6.0 ACKNOWLEDGMENTS

7.0 REFERENCES

[1]   2008. Petroleum Quality Information System Report, Defense Energy Support Center - DESC-BP. Fort Belvoir Virginia.

[2]   Report of the Defense Science Board Task Force on DoD Energy Strategy "More Fight-Less Fuel." Office of the Under Secretary of Defense For Acquisition, Technology, and Logistics, Washington, D.C. February 2008.

[3]   P. Roberts, National Geographic (2008).

[4]   K. S. Deffeyes "Beyond Oil: The View from Hubbert's Peak," Hill and Wang: 2005.

[5]   T. Coffey, D.R. Hardy, G.E. Besenbruch, K.R. Schultz, L.C. Brown, and J.P. Dahlburg, Defense Horizons 36 (2003) 1.

[6]   H.R.6:   Energy   Independence   and   Security   Act   of   2007. http://en.wikipedia.org/wiki/Fredom_Act. Last accessed May 8, 2008.

[7]   K.Y. Vinnikov, A. Robock, R.J. Stouffer, J.E. Walsh, C.L. Parkinson, D.J. Cavalieri, J.F.B. Mitchell, D. Garrett, and V.F. Zakharov, Science 286 (1999) 1934-1937.

[8]   G.A. Olah, A. Goeppert, and G.K.S. Prakash, Beyond Oil and Gas: The Methanol Economy. Wiley-VCH Verlag GmbH & Co. KGaA, Weinheim, 2006.

[9]   V. Nikulshina, C. Gebald, and A. Steinfeld, Chemical Engineering Journal 146 (2009) 244-248.

[10]   J.P. Collin, and J.P. Sauvage, Coordination Chemistry Reviews 93 (1989) 245-268.

[11]   E. Fujita, Y. Hayashi, S. Kita, and B.S. Brunschwig, Carbon Dioxide Utilization for Global Sustainability 153 (2004) 271-276.

[12]   H. Noda, S. Ikeda, Y. Oda, K. Imai, M. Maeda, and K. Ito, Bulletin of the Chemical Society of Japan 63 (1990) 2459-2462.

[13]   W.W. Russell, and G.H. Miller, Journal of the American Chemical Society 72 (1950) 2446-2454.

[14]   R.W. Dorner, D.R. Hardy, F.W. Williams, B.H. Davies, and H.D. Willauer, Energy & Fuels (submitted).

[15] T. Riedel, G. Schaub, K.W. Jun, and K.W. Lee, Industrial & Engineering Chemistry Research 40 (2001) 1355-1363.

[16] J. Laugier, and B. Bochu. 2003. Celref. Can be obtained off the web at the LMGP (Laboratoire des Materiaux et du Ge′nie Physique de I′Ecole Supe′rieure de Physique de Grenoble http://www.inpg.fr/LMGP/) program suite site at http://www/ccp14.ac.uk/ccp/web-mirrors/lmgp-laugier-bochu/

[17] R. Hesse, T. Chasse, and R. Szargan, Analytical and Bioanalytical Chemistry 375 (2003) 856-863.

[18] L.Y. Xu, Q.X. Wang, D.B. Liang, X. Wang, L.W. Lin, W. Cui, and Y.D. Xu, Applied Catalysis a-General 173 (1998) 19-25.

[19] P.H. Choi, K.W. Jun, S.J. Lee, M.J. Choi, and K.W. Lee, Catalysis Letters 40 (1996) 115-118.

[20] J.S. Kim, S. Lee, S.B. Lee, M.J. Choi, and K.W. Lee, Catalysis Today 115 (2006) 228-234.

[21] T. Riedel, M. Claeys, H. Schulz, G. Schaub, S.S. Nam, K.W. Jun, M.J. Choi, G. Kishan, and K.W. Lee, Applied Catalysis a-General 186 (1999) 201-213.

[22] M.D. Shroff, D.S. Kalakkad, K.E. Coulter, S.D. Kohler, M.S. Harrington, N.B. Jackson, A.G. Sault, and A.K. Datye, Journal of Catalysis 156 (1995) 185-207.

[23] E.S. Lox, and G.F. Froment, Industrial & Engineering Chemistry Research 32 (1993) 71-82.

[24] S.Z. Li, S. Krishnamoorthy, A.W. Li, G.D. Meitzner, and E. Iglesia, Journal of Catalysis 206 (2002) 202-217.

[25] M.R. Goldwasser, V.E. Dorantes, M.J. Perez-Zurita, P.R. Sojo, M.L. Cubeiro, E. Pietri, F. Gonzalez-Jimenez, Y.N. Lee, and D. Moronta, Journal of Molecular Catalysis A-Chemical 193 (2003) PII S1381-1169(1302)00472-00477.

[26] D.B. Bukur, L. Nowicki, R.K. Manne, and X.S. Lang, Journal of Catalysis 155 (1995) 366-375.

[27] J. Abbot, N.J. Clark, and B.G. Baker, Applied Catalysis 26 (1986) 141-153.

[28] T.Z. Li, Y. Yang, C.H. Zhang, X. An, H.J. Wan, Z.C. Tao, H.W. Xiang, Y.W. Li, F. Yi, and B.F. Xu, Fuel 86 (2007) 921-928.

[29] J.B. Butt, Catalysis Letters 7 (1990) 61-82.